A Quantitative Framework to Assess Hydrologic Connectivity

Alexander Brooks[1], Tim Covino[1], and Ed Hall[1]

[1]Colorado State University

November 30, 2022

Abstract

Water-mediated linkages that connect landscape components are collectively referred to as hydrologic connectivity. These linkages influence numerous watershed processes including biogeochemical cycling, spatial vegetation patterns, and stream runoff generation. The concept of hydrologic connectivity also informs environmental management and underpins regulations protecting waterways. However, to date, there is no consensus on how to quantitatively assess connectivity. Here, we develop and test a framework to quantify hydrologic connectivity within a landscape. We define connectivity as a continuous variable (from 0 to 1) that represents the vector strength between any two points in the landscape (a source to a target). To measure this vector strength, we analyzed hydrologic and geochemical indicators within a montane river-floodplain system across a dynamic range of streamflows. In addition to applying hydrologic and geochemical indicators, we tested the ability of microbiome membership to provide further insight into connectivity dynamics. From these data, we generated complementary time series of lateral connectivity (between the river and the floodplain) and longitudinal connectivity (along the river from upstream to downstream). We then quantified key parameters associated with connectivity regimes among waterbodies including connectivity strength and stability, and timing and speed of changes in connectivity. The application of a microbial index for connectivity provided new insight into flowpath residence times that was not apparent using more traditional hydro-geochemical approaches. The proposed connectivity framework moves beyond binary qualitative descriptions of connectivity and provides a coupled conceptual and empirical approach to quantify the spatiotemporal variability of hydrologic connectivity.

A Quantitative Framework to Assess Hydrologic Connectivity

Alexander C. Brooks [1,3]
Tim Covino [1,2,3]
Ed K. Hall [2,3]

1. Department of Geosciences, Colorado State University, Fort Collins, Colorado, 80524, USA

2. Department of Ecosystem Science and Sustainability, Colorado State University, Fort Collins, Colorado, 80524, USA

3. Natural Resources Ecology Laboratory, Colorado State University, Fort Collins, 80524, USA

Corresponding Author: Alexander C. Brooks, 617-922-7289, alex.brooks@colostate.edu

Keywords:

Hydrologic connectivity, microbiology, floodplain, river-floodplain connectivity

1. Abstract

Water-mediated linkages that connect landscape components are collectively referred to as hydrologic connectivity. These linkages influence numerous watershed processes including biogeochemical cycling, spatial vegetation patterns, and stream runoff generation. The concept of hydrologic connectivity also informs environmental management and underpins regulations protecting waterways. However, to date, there is no consensus on how to quantitatively assess connectivity. Here, we develop and test a framework to quantify hydrologic connectivity within a landscape. We define connectivity as a continuous variable (from 0 to 1) that represents the vector strength between any two points in the landscape (a source to a target). To measure this vector strength, we analyzed hydrologic and geochemical indicators within a montane river-floodplain system across a dynamic range of streamflows. In addition to applying hydrologic and geochemical indicators, we tested the ability of microbiome membership to provide further insight into connectivity dynamics. From these data, we generated complementary time series of lateral connectivity (between the river and the floodplain) and longitudinal connectivity (along the river from upstream to downstream). We then quantified key parameters associated with connectivity regimes among waterbodies including connectivity strength and stability, and timing and speed of changes in connectivity. The application of a microbial index for connectivity provided new insight into flowpath residence times that was not apparent using more traditional hydro-geochemical approaches. The proposed connectivity framework moves beyond binary qualitative descriptions of connectivity and provides a coupled conceptual and empirical approach to quantify the spatiotemporal variability of hydrologic connectivity.

2. Significance Statement

Hydrologic connectivity has become an important conceptual framework for understanding how the movement of water influences landscape scale processes. Despite this popularity, we currently lack a standardized quantitative approach for measuring connectivity. Historically, the most common approach has been to measure only the presence or absence of connectivity. In this paper, we provide a new framework of connectivity that quantifies connectivity between locations as a continuous metric that can vary in magnitude both in space and time, and be derived using field indicators. We further, develop a new technique for measuring connectivity using water-column microbiomes, which provide an information dense tracer that integrates information about water sources and travel times in landscapes.

3. Introduction

Hydrologic linkages of matter and energy within landscapes are important regulators of physical (1), biogeochemical (2) and biological processes (3). These linkages, defined as hydrologic connectivity, are a fundamental landscape property that connect multiple watershed components (e.g., uplands, streams, floodplains, hyporheic zones, groundwater) that emerge from interactions of topographic, climatic, geologic, biotic,

and anthropogenic controls (4). Hydrologic connections operate simultaneously across multiple dimensions: vertical (surface-groundwater), lateral (river-floodplain & river-hillslope), longitudinal (upstream to downstream), and temporal (5). The magnitude and directionality of connectivity can vary depending on the spatial and temporal scale being considered (2). Equally as important as identifying when surface water features are connected is identifying when they are not connected, known as disconnectivity or isolation, which plays a critical role in a suite of important hydrologic and biogeochemical processes (6, 7) and in the maintenance of habitat complexity and biodiversity (3). For example, isolated wetlands, or wetlands with no surface water connection to the stream network, have been shown to control water quality (8) and regulate streamflow (9) at regional to continental extents.

3.1 Quantifying Hydrologic Connectivity

Quantifying hydrologic connectivity reveals how physical landscape features are connected through space and time. The physical template that determines potential connectivity pathways is known as structural connectivity (10). However, for hydrologic connectivity (hereafter connectivity) to be achieved, flow must overcome resistance, impedances, and losses along those pathways (11). Thus, connectivity may only occur under specific hydrologic conditions driven by internal (e.g., soil moisture conditions) and external (e.g., precipitation or snowmelt) factors (12). Assessing connectivity requires a framework that can quantify the degree to which material and energy moves among landscape components (1, 13). Common field methods to measure connectivity include hydrologic measurements (e.g., soil moisture, water levels, streamflow), geochemical and isotopic end-member mixing analysis and conservative tracer experiments (14–16). However, different measurements provide information about different aspects of connectivity and are often only applicable at specific spatial or temporal scales, hindering between study comparisons and therefore the direct translation of connectivity assessments to policy and management decisions (17).

3.1.1 Incorporating Microbial Indicators of Hydrologic Connectivity

A useful synthetic framework should be able to incorporate information from multiple sources including emerging approaches such as microbial indicators of connectivity. Recent work has demonstrated that analysis of microorganisms can be a valuable tool in hydrologic research because membership of aquatic microbiomes are intimately coupled with hydrologic processes (18–20). Microorganisms are generally passive dispersers in aquatic systems and dispersal effects are primarily driven by the directional flow of water (21). As a result, downstream aquatic microbiomes have been shown to be similar to the microbiomes within shallow soils (22) and deeper groundwater (23) that generate streamflow. However, as surface water ecosystems become disconnected and residence times of those systems increase, community assembly is increasingly affected by ecological dynamics (e.g. competition, predation) that result in changes in the local microbiome (22, 24). At any one point in time, aquatic microbiome membership is the balance between immigration and emigration, which are

primarily controlled by hydrologic flow states and aquatic network structure, and microbial growth and mortality, which are affected by *in situ* environmental drivers (e.g., resources and temperature) (25–27). As hydrologic flow states and aquatic network structure also influence hydrologic connectivity, the membership of aquatic microbiomes has the potential to reflect connectivity status. The recent advances in analytical techniques and bioinformatic pipelines to characterize the microbiome have made analyses of environmental microbiomes both affordable and accessible (28). These increasingly commonplace analyses of microbiomes coupled with the ubiquity of microorganisms, make microbial analyses a potentially powerful tool for assessments of hydrologic connectivity at a wide range of temporal and spatial scales. To assess microbiome membership as a potential indicator of connectivity, we also characterized microbiome membership over the course of a seasonal hydrograph within our connectivity framework.

4. Hydrologic Connectivity Framework

To quantify hydrologic connectivity, we first identified a source site and consider the magnitude of connectivity between this source and multiple target sites. The magnitude of this connectivity can vary over short timescales (hours to seasons) as hydrologic and environmental conditions change through time (12). The long-term (years to decades) patterns of shifts in connectivity depend on both landscape structure and local hydro-climatic regimes. Some fluvial landscapes can exhibit stable connectivity over years to decades. For example, a spring fed stream with constant discharge is strongly connected to the originating spring whereas a geographically isolated wetland might never have surface connectivity with rivers in the same watershed. However, many landscapes often exhibit more dynamic connectivity in time and/or across spatial gradients. For example, hydrologic connectivity between upland portions of the landscape to the river network is heterogeneous in time and space and is controlled by wetness patterns and watershed morphology (29, 30). In high-relief landscapes, spatial patterns of watershed hydrology (e.g., soil moisture and groundwater) are often organized by watershed topography. For example, water tends to concentrate in hillslope valley bottoms and these landscape positions can be hydrologically connected to the river corridor for large portions of the year (31). Conversely, the ridgetops between valley bottoms, tend to shed water and may only connect to the river corridor during the wettest periods. Similarly, rivers connect and disconnect to different parts of their floodplains during hydrologic events based on flood hydraulics and river-floodplain geomorphology. High physical complexity in floodplain systems creates heterogeneity in connectivity across the landscape that can be the principal driver of many of the characteristic riparian ecological processes (32, 33).

While connectivity can be considered as a binary attribute, (i.e., the presence or absence), here, we define the connectivity magnitude as connectivity strength (σ) and quantify this as a continuous variable ranging from 0 and 1. Connectivity strength denotes the degree of influence of the source on the target. To measure connectivity strength, we assumed that when strong hydrologic connectivity was present, source and

target water compositions would be more similar than when connectivity was weak or absent. This is a commonly used assumption embedded in source water mixing approaches which use aqueous geochemistry to assess hydrologic connectivity (15, 34). For microbial communities, we expected that when hydrologic connectivity was strong, the membership of the water column microbiome would be more similar because the target community would be strongly influenced by immigration from the source community. Conversely, when hydrologic connectivity was weak/absent, we expected inter-species interactions would be the dominant influence on microbiome membership and the source and target would become less similar over time. Using this approach we generated time series of connectivity strength (σ) that enabled us to consider both spatial and temporal connectivity to define a landscape's connectivity regime.

To test our framework's ability to describe spatiotemporal patterns of connectivity, we focused on measuring hydrologic connectivity among multiple surface water features of a montane floodplain. We combined data from a network of high frequency water level sensors and flow tracer injections with weekly sampling for aqueous geochemistry and microbiome membership. We collected individual samples for aqueous geochemistry and microbiome membership at eleven sites over the course of a single season's hydrograph. A single sampling site along the main river channel at the inflow of the river-floodplain was defined as our "source" site and the other 10 sites served as "target" sites within the context of our framework (Figure 1B). We used this experimental design to test the proposed framework including generating a time series of connectivity strength and quantifying a range of connectivity attributes including the stability, timing and spatial structure of hydrologic connections within the floodplain.

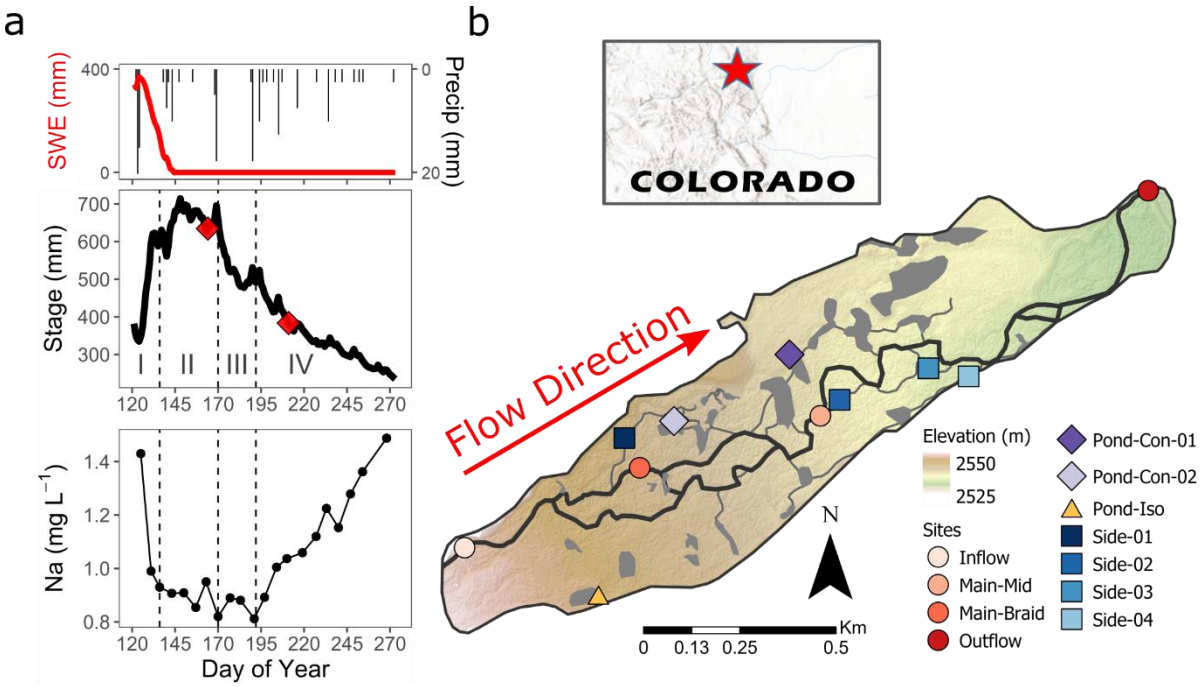

Figure 1: (a) Hyetograph (from SNOTEL #1042), stage and sodium (Na) concentrations at inflow site and (b) North St Vrain river-floodplain map. Red line in (a) is snow water equivalent (SWE), red diamonds in (a) indicate dates of tracer injection experiments. River flows hydro periods are categorized as (I) rising limb, (II) peak flows, (III) falling limb, and (IV) recession. Map shows simplified depiction of surface water major river braids (dark grey) and floodplain surface features including ponds, wetlands and side channels (lighter grey).

5. Methods

5.1 Field Sample Collection and Lab Analysis

We collected weekly water samples from May 05, 2018 to September 25, 2018 at a total of eleven surface water sites within a river-floodplain system along the North St. Vrain River, Colorado (Figure 1). The river has a snowmelt driven hydrograph with late spring/early summer snowmelt peak flows and summer streamflow recession (35). The river has a multi-thread planform within the river-floodplain system. There were four sampling sites along the river including at the upstream (Inflow) and downstream (Outflow) boundaries of the river-floodplain reach and along two major channel threads within the river-floodplain system (Main-Mid & Main-Braid). The floodplain has high spatial heterogeneity and a mosaic of ponds, side channels and wetlands (36). To capture this heterogeneity, we included four side channel sites (Side-01 to Side-04), two connected pond sites that had an upstream surface connection to the river (Pond-Con-01 & Pond-Con-02) and one isolated pond (Pond-Iso) with no surface channel

connection to the river. All sites were sampled weekly throughout the study period for a total of 21 sampling events.

A total of 227 water samples were collected for aqueous geochemistry, filtered within 24 hours with a 0.45-µm PVDF filter (Millipore, HVLP04700) and frozen until analysis for major ions using a Dionex ICS-3000 ion chromatograph at the US Forest Service Rocky Mountain Research Station in Fort Collins, Colorado. A subset of 215 water samples from May to September were collected in sterile 60 mL falcon tubes for 16S rRNA amplicon analysis, kept cold until filtered within 12 hours onto a white polycarbonate GTTP 0.2-µm filter (Millipore, GTTP02500), flash frozen with liquid nitrogen and then stored in a -80°C freezer until analysis. To assess within site variability, for a subset of sites (Inflow, Outflow, Side-01, Pond-Con-01, and Main-Mid), we collected duplicate samples each week. At all other sites, only individual samples were collected.

We extracted DNA from each filter with a MoBio PowerSoil® DNA Isolation Kit using standard protocols. The 16S rRNA gene (V4 region) was amplified using 515F and 806R universal primers with the forward primer barcoded following the Earth Microbiome Project protocols (37). The forward primer 515F included the unique sample barcode following Parada et al. 2016 (38) and both primers included degeneracies as described in Parada et al. 2016 and Apprill et al. 2015 (39). For each sample, we ran a 50 µL PCR reaction using an Invitrogen PlatinumTM Hot Start PCR Master Mix with 10 µL of DNA. The PCR product was quantified and then pooled into a single pool in equimolar concentrations and cleaned using a MinElute® PCR Purification kit. Cleaned, pooled DNA was sequenced with a MiSeq reagent v2 500 cycle kit on the Illumina MiSeq platform at the Colorado State University Next Generation Sequencing Core facility. Sequence reads were analyzed using MOTHUR (40) and OTU counts defined at a 97% similarity of the sequence using the OptiClust algorithm. Generated OTUs were then aligned to a SILVA reference file (41).

5.2 Hydrometric Field Measurements and Conservative Tracer Injection

At all sites, we monitored water level at 15 minute intervals for the duration of the study using either TruTrack Capacitance Rods or HOBO U20L Pressure Transducers. To capture relative stage dynamics, we standardized mean daily stage as a z-score by normalizing mean daily stage by the seasonal mean and standard deviation of water levels across the period of record at each individual site. Precipitation and snow water equivalent records were downloaded from the Wild Basin SNOTEL, #1042, (2914 m), located within the watershed.

To determine how river-floodplain connectivity changed as a function of streamflow we conducted instantaneous NaCl injection experiments at high (June 13, 2018) and intermediate flows (July 30, 2018) at a site on the main stem 125m above the Inflow site. The change in injected tracer concentration through time (i.e., tracer breakthrough

curve) was measured at six sites (Table 1) using Campbell CS547A-L conductivity loggers and background corrected using pre and post-injection measurements. Time to peak (TTP) was measured as the time from injection to peak conductivity at a site and modal velocity (V_m) was calculated as the estimated flow path distance from the injection site ($DIST_f$) divided by the TTP.

Table 1: Tracer experiment results at target sites for high and intermediate flow NaCl tracers injected at the Inflow site. NR indicates that no tracer arrival was observed at the target site.

					High Flow (June 13, 2018)		Intermediate Flow (July 30, 2018)	
				Inflow Stage (mm:):	635		384	
Site	Site Type	Elev (m)	Surface Connection to Inflow	DISTf[1] (m)	TTP[2] (min)	Vmod[3] (m/s)	TTP[2] (min)	Vmod[3] (m/s)
Outflow	Major Channel	2535	Yes	2228	46	0.78	85	0.43
Main-Mid	Major Channel	2543	Yes	1175	23	0.87	41	0.48
Side-01	Side Channel	2548	Yes	607	35	0.29	NR	NR
Pond-Con-01	Connected Pond	2542	Yes	1040	196	0.09	NR	NR
Pond-Con-02	Connected Pond	2545	Yes	734	101	0.12	NR	NR
Pond-Iso	Isolated Pond	2550	No	-	NR	NR	NR	NR

1) Estimated surface flow path distance from the injection site. Note there is no surface channel connection between Inflow and the Isolated Pond (Pond-Iso)
2) Time to Peak
3) Modal Velocity – calculated as DISTf / TTP

5.3 Connectivity Strength Metrics

To calculate connectivity strength using aqueous geochemistry, we first normalized ion concentrations by their mean and standard deviations and conducted a principle component analysis (PCA) on all major ions present including sodium, chloride, calcium, magnesium, potassium and sulfate ions. Analytical results included several outlying values for chloride and potassium that were removed due to suspected contamination. To maintain a balanced dataset, these values were replaced with linearly interpolated values using reported values from the previous and subsequent weeks at the same site. We examined PCA eigenvalues and eigenvectors (Table S1), and based on variable loadings, we chose to include two principle components (PCs) for further

analysis that represented two major water source components. At each sampling date, within the 2 dimensional PC space (PC1 and PC2), the log transformed Euclidean distance was calculated between a given target site geochemical composition and the composition at the Inflow (i.e., source site) (Eq. 2). This value was then rescaled to between 0 and 1 using a min-max normalization and reversed to calculate a chemical similarity score as follows (Eq. 1 & 2).

$$ED_i = log\left(\sqrt{(PC1_{s_i} - PC1_{t_i})^2 + (PC2_{s_i} - PC2_{t_i})^2}\right) \quad \text{(Eq. 1)}$$

$$\sigma_i = 1 - \left(\frac{ED_i - \min(ED)}{\max(ED) - \min(ED)}\right) \quad \text{(Eq. 2)}$$

Where ED_i is the logged Euclidian distance within the PCA space at a given sampling date, the subscripts s_i and t_i refer respectively to PC scores at the Inflow site and a target site, σ_i is the connectivity strength at a given sampling date and ED is the complete dataset.

To calculate connectivity strength using microbiome membership, we first removed samples with limited sequences (<1000 reads), trimmed operational taxonomic units (OTUs) to remove samples not observed more than 3 times in 20% of the samples, and relativized OTU counts by the total OTUs in the sample. All 16S amplicon analyses were conducted using the phyloseq package in R (42). Due to lack of duplication at all sites, we further merged duplicate samples into mean values to simplify subsequent analysis. On each sample date, we calculated a similarity score using the Bray-Curtis similarity index (BC) between a given site (i.e., target) and the inflow (i.e., source), as follows (Eq. 3).

$$BC_{st} = \frac{2C_{st}}{S_s + S_t} \quad \text{(Eq. 3)}$$

Where C is the sum of the lesser counts of OTUs found at both sites while S_s is the total number of sequence reads at the Inflow site and S_t is the total number of sequence reads at the target site. We also conducted a principle coordinate analysis (PCOA) using the BC dissimilarity index to visualize microbiome membership in lower dimensional space.

5.4 Logistic Curve Fitting

To better understand hydrologic connectivity dynamics at our field system, we evaluated connectivity data across the hydrograph from peak to low flow conditions (May 16, 2018 – Sep 25, 2018). During this period, we posited that connectivity strength (σ) between the inflow and river-floodplain sites could either be stable or shift from high to low connectivity strength states, and therefore be represented by a sigmoidal function, here described in the form of a four parameter logistic function. Using the drc package in R (43), we fit a four parameter logistic equation to our connectivity strength timeseries

derived from both geochemical composition and microbial membership, as follows (Eq. 4).

$$\sigma = c + \frac{d - c}{1 + \exp(v * (t - e))} \qquad \text{(Eq. 4)}$$

Where σ is the connectivity strength, *d* is the upper asymptote, *c* is the lower asymptote, *v* is the slope at the inflection point, *t* is time, and *e* is the value of *t* when σ is halfway between *d* and *c* (Table 2). The difference between *d* and *c* describes the change in the magnitude of connectivity strength (Δ). When the system is stable, (Δ = 0), σ = *d* = *c*. When there is a change in connectivity strength (Δ > 0), then the value *e* can be used to describe the timing of this change and *v* describes the speed of the change (Table 2). To identify if the logistic fit was an appropriate model over our seasonal timescale, we compared the root mean square error of the residuals (RMSE) to that of a null model represented by the horizontal line σ = *a* where *a* was the mean value of σ across the time period. We then compared parameter estimates from the logistic fit between metrics and between sites and assessed their uncertainty using each parameter's standard errors and p-values.

Table 2: Connectivity regime parameters and associated symbols.

Connectivity Regime Parameters	**Parameter Symbol**
Connectivity Strength	σ
Timescale	*t*
Magnitude of Changes in Connectivity Strength	Δ
Timing of Changes in Connectivity Strength	*e*
Speed of Changes Connectivity Strength	*v*
Maximum Connectivity Strength	c (max)
Minimum Connectivity Strength	d (min)

6. Results

6.1 Hydrometric Monitoring and Tracer Experiment:

Stream levels in the North St Vrain River followed a seasonal pattern consistent with snow driven hydrographs of the Southern Rockies with rising streamflow starting in late April, peak flows in late May to early June and falling streamflow throughout the summer (Figure 1A). Several summer convective storm events occurred in July and August but did not strongly influence the seasonal hydrograph (Figure 1A). Using stage and geochemical patterns at the Inflow (Figure 1A), we categorized four distinct hydro periods: (I) rising limb (May 01, 2018 – May 15, 2018); (II) peak flow (May 16, 2018 – June 18, 2018); (III) falling limb (June 19, 2018 – July 10, 2018); and (IV) recession (July 11, 2018 – Sept 30, 2018) (Figure 1). Analysis of patterns in standardized mean daily stream levels indicated strongly coherent hydrologic dynamics at the major channel sites while floodplain sites followed the broad seasonal pattern of the Inflow site but also demonstrated distinct site specific behavior (Figure 2).

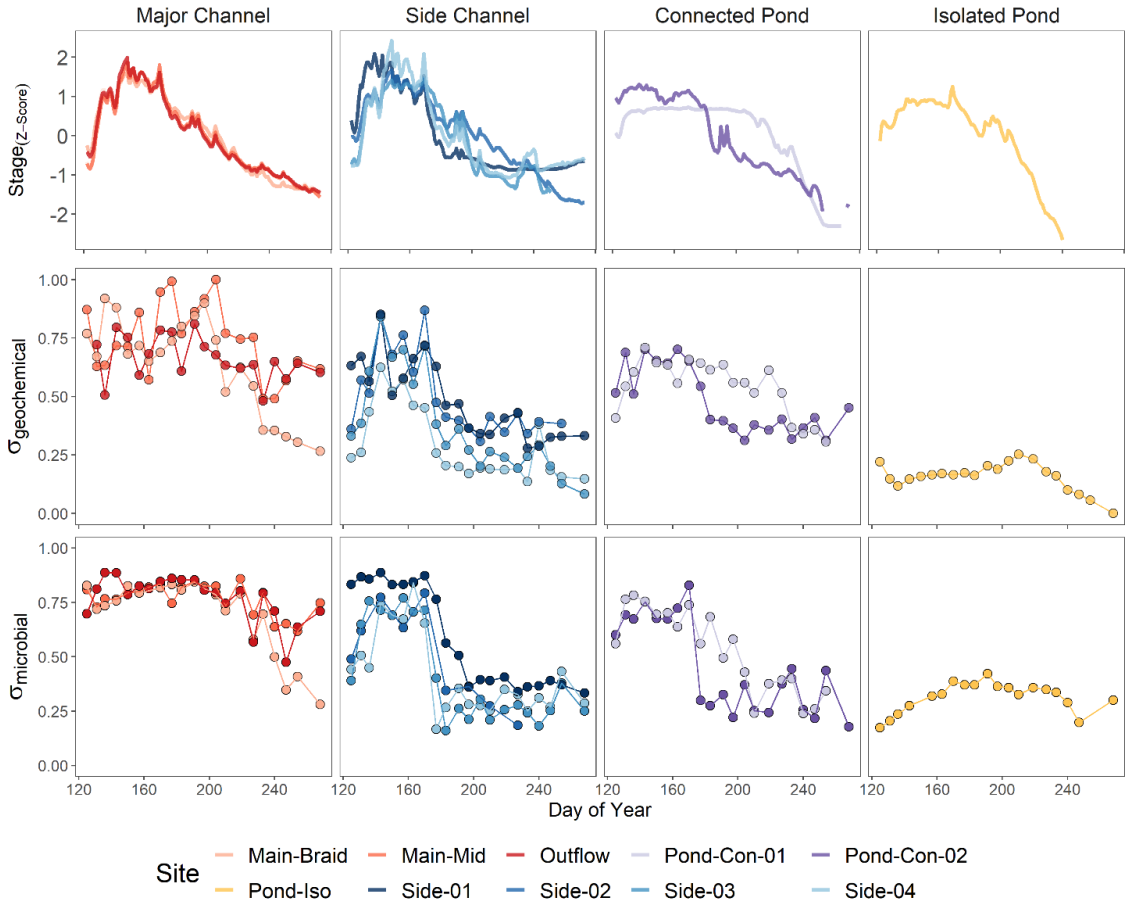

Figure 2: Time series of relative stage (top row) and connectivity strength (σ) using geochemical (middle row) and microbial (bottom row) metrics. Stage values are standardized as normalized by the mean and standard deviation across the period of record at each site.

At side channel sites (Figure 1B), water levels followed similar patterns to the main channel during the rising limb and peak flows (Figure 2). During the falling limb and into the recession, water levels at the side channels generally exhibited a steep drop and were subsequently less responsive to main channel level fluctuations. Both of the surface connected ponds (Pond-Con-01 & Pond-Con-02) and the isolated pond (Pond-Iso) had high water levels starting in May that plateaued for much of the season before declining during the falling limb at Pond-Con-02 and during the recession at Pond-Con-01 and Pond-Iso (Figure 2). The high water levels in pond sites during the rising limb suggest sampling began after ponds had already mostly filled with groundwater, local snowmelt, and streamwater. Pond-Con-01 and Pond-Cond-02 went dry in mid-September while at Pond-Iso, levels dropped below our water level logger in early September and the pond went completely dry in late September (Figure 2).

The tracer injection experiments conducted during high (June 13, 2018) and intermediate flows (July 30, 2018) demonstrated the presence or absence of surface water connectivity between Inflow and a subset of target sites (Table 1). We did not observe arrival of injected tracer at Pond-Iso during either experiment, providing strong evidence of a lack of surface connectivity between these sites (Table 1). Tracer arrivals at other sites were variable, and we only observed tracer arrival during both the high and intermediate flow injections at the Major Channel sites (Table 1). During the high flow tracer injection, tracer arrival was first observed at Main-Mid with a time to peak (TTP) of 22.5 minutes, followed by Side-01 (TTP: 35 min), Outflow (TTP: 46 min) and a more attenuated response at Pond-Con-02 (TTP: 101 min) and Pond-Con-01 (TTP: 196 min) (Table 1). Modal velocity, which is defined as the most common velocity along a flowpath, was highly variable at connected sites (range: 0.09 - 0.87 m s^{-1}, Table 1) indicating variable residence times along connected flow pathways. During the intermediate flow tracer, the tracer arrival was only observed at the Main-Mid site (TTP: 40.8 min, $Vel_{m:}$ 0.48 m s^{-1}) and Outflow site (TTP: 85 min, $Vel_{m:}$ 0.43 m s^{-1}). As tracer injections cannot detect flowpaths with residence times longer than the window of detection, the lack of response at Side-01, Pond-Con-01 and Pon-Con-02 during the intermediate flow injection can't confirm a complete absence of surface connectivity. However, these results do demonstrate that sites were not strongly connected with the Inflow site.

6.2 Seasonal Dynamics in Aqueous Geochemical and Microbial Composition

We conducted a principal component analysis to see which geochemical indicators were most indicative of connectivity. The primary principal component (PC1) corresponded to bulk ionic strength and explained 62.2% of variance and the secondary principal component (PC2) explained 17.8% of variance and was strongly driven by SO_4^{2-} concentrations (Table S1). All ion concentrations were negatively related to PC1 with Na^+, Ca^{2+}, Cl^-, Mg^{2+}, and K^+ having moderate loadings (between -0.39 to -0.48).

382 SO_4^{2-} had a strong positive loading on PC2 (0.84) while $Ca^{2+}$and Mg^{2} had moderate negative loadings (-0.36 and -0.30, respectively).

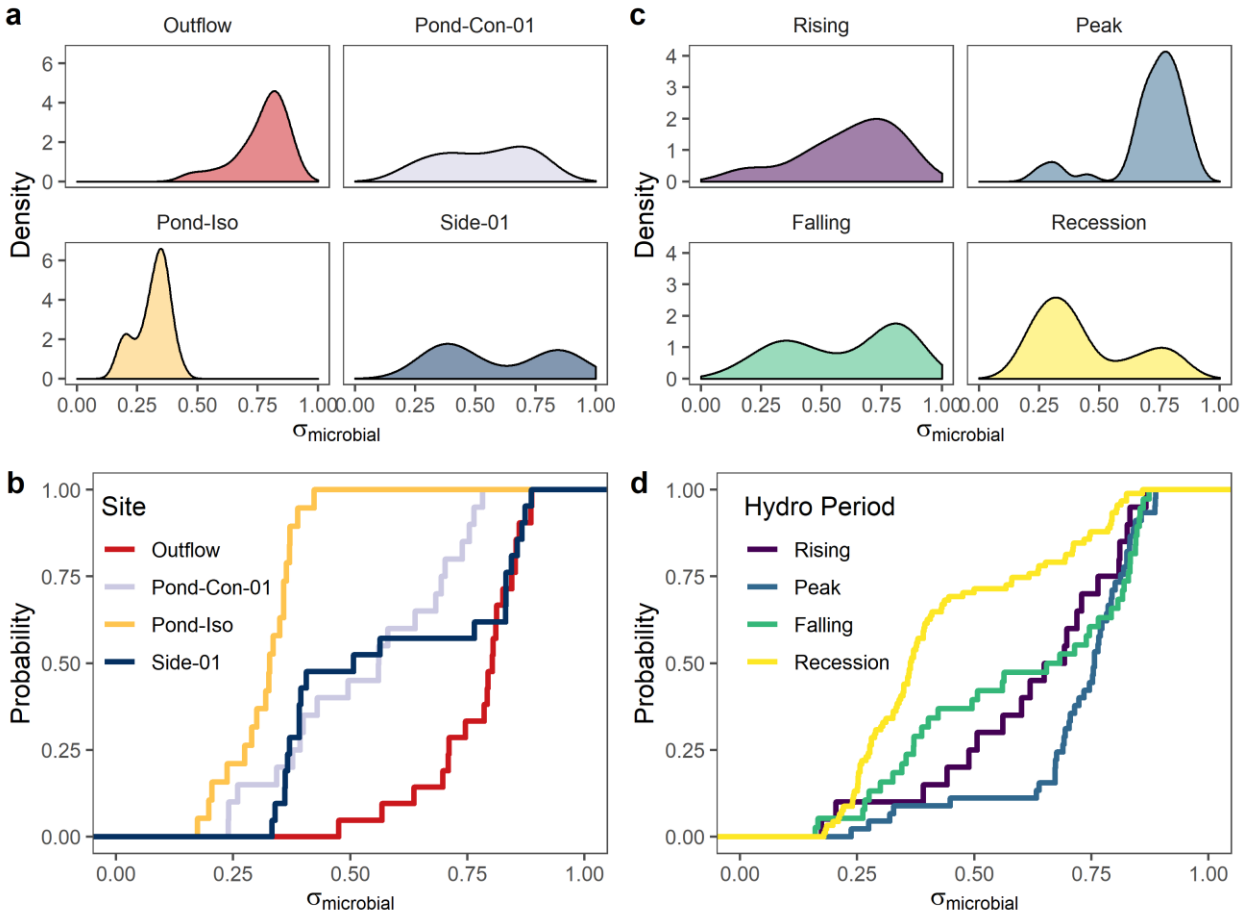

384

386 **Figure 3:** Temporal (a, b) and spatial (c,d) density plots and empirical cumulative distribution functions of connectivity strength (σ) between the Inflow site and target sites as derived from microbial membership. Temporal plots (a, b) show results from four 388 target sites with distinct connectivity regimes through the full study period. Stable connectivity regimes tended toward unimodal distributions (eg. Outflow & Pond-Iso) with 390 relatively low spread while sites with intermittent connectivity exhibited both strong (Side-01) and weak (Pond-Con-01) bimodality with broader distributions. Spatial plots 392 (c,d) are aggregates of all sites by hydro period and illustrate shifting spatial patterns of connectivity within the river-floodplain system over varying hydrologic conditions. Peak 394 river stage resulted in a high density of high σ values and low river stage during the recession had a bimodal distribution with a dominant modal peak at low σ values. 396 Intermediate river stage during the falling limb exhibited a more dampened bi-modal distribution with increased overall heterogeneity throughout the river-floodplain system.

398

Seasonal geochemical patterns at the Inflow site followed a snowmelt dilution pattern 400 where geochemical ion concentrations (e.g., Na^{+}) were lowest during peak flows (Figure

1A, S3). This geochemical pattern propagated strongly to sites with surface connections to the river during high flows resulting in high peak connectivity strength scores (Figure 2 & 3). At lower flows, geochemical composition diverged between the Inflow site and the floodplain sites, resulting in lower connectivity strength scores (Figure 2 & 3). Pond-Iso had distinct geochemistry from the Inflow throughout the season resulting in low connectivity strength scores across the study period. (Figure 2).

We conducted a principal coordinates analyses (PCOA) to explore season dynamics in microbiome membership and identify microbiome membership's utility as an indicator of connectivity. The PCOA of microbiome membership identified a major axis PCOA-1 that explained 33.7% of the variance in microbiome membership and a secondary axis that explained 16.1% of the variance (Figure S1). Additional axes all explained less than 10% of the variance. Microbial membership at the Inflow site shifted slightly between the rising limb and falling limb with the highest variation observed during the recession period (Figure S2). During peak flows, sites with surface connections to the river had microbiomes similar to Inflow, resulting in high connectivity strength scores (Figure 2 & 3, Figure S2). Major channel sites maintained their similarity to the Inflow for most of the study period with some divergence in the late recession. At side channels and connected pond sites, microbiome membership started diverging from the seasonal pattern at Inflow in either the falling limb or recession, resulting in lower connectivity strength scores later in the season (Figure 2 & 3). As with its geochemistry, Pond-Iso had distinct microbial membership from the Inflow site throughout the season that remained relatively stable resulting in low connectivity strength scores across the study period (Figure 2 & 3).

6.3 Connectivity Shifts: Strength, Timing and Speed

Parameters derived from the logistic fit to the connectivity strength time series (from peak flow through the recession) revealed divergent patterns among sites with differences in both the timing and magnitude of changes in connectivity strength. All sites had low to moderate root mean square error (RMSE) for the logistic fit (geochemical metric RMSE: 0.035 to 0.127, microbial metric RMSE: 0.033 to 0.102), which at all sites was lower than for the null model (Table S2). However, there were two cases where the logistic fit was only marginally better than the null model. This was true at Pond-Iso for the microbial metric (RMSE difference of 0.004) and at the Outflow site for the geochemical metric (RMSE difference of 0.006).

We used the model to assess the magnitude (Δ), timing (*e)* and speed (*v)* of connectivity changes at all sites. In general there was strong agreement for magnitude ($r = 0.77$) and timing ($r = 0.82$) between parameters estimated by the geochemical metric and those estimated by microbial metric but weak agreement between metrics for the speed parameter ($r= 0.25$) (Figure 4). Magnitudes of changes were low at the isolated pond and sites along the main channel (Δ_g (aqueous geochemistry) range: 0.09

– 0.24, Δ_m (microbial) range: 0.14-0.21) and higher at all other sites where Δ_g ranged from 0.27 to 0.51 and Δ_m ranged from 0.39 to 0.53 (Figure 4, Table S3, S4). All side channels and Pond-Con-02 shifted connectivity states during the falling limb with shift timing ranging from day of year (doy) 173-178 for e_g (aqueous geochemistry) and doy 172-183 for e_m (microbial) while major channel sites shifted later on the hydrograph recession (e_g 210-228, e_m 217-238). Despite the general agreement between both metrics for e, there was a large difference at Pon-Con-01 where the microbial metric revealed a connectivity change occurring 40 days prior to a detectable change from the geochemical metric. The maximum speed of connectivity changes as derived from the scalar parameter v also exhibited variable behavior between sites but had high parameter uncertainty, particularly for sites with higher speeds. However, for several sites that had lower speeds (v <0.25), parameter uncertainty was low and the microbial and geochemical metrics were in better agreement.

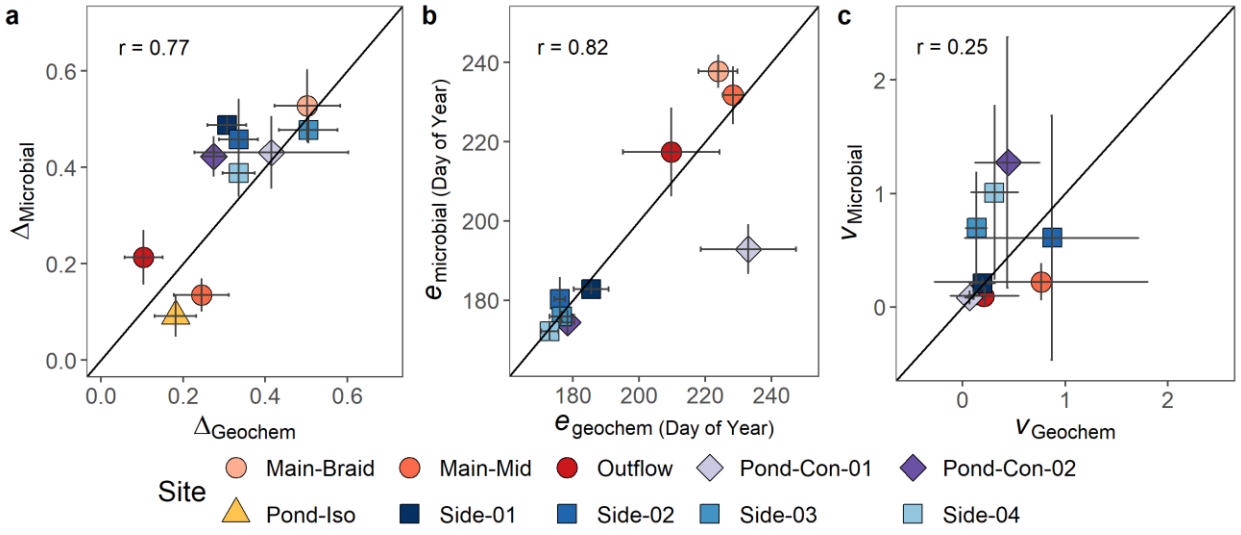

Figure 4: Connectivity parameter values derived from logistic curve fitting from peak to recession hydro period including (a) Connectivity change magnitude (Δ), (b) connectivity change timing (*e)*, and (c) connectivity change speed (*v*). Black line denotes 1:1 between parameter values derived from geochemical and microbial metrics. Error bars denote standard errors. Parameters were moderately to strongly correlated between metrics for connectivity change magnitude and timing but weakly correlated for the connectivity change speed.

7. Discussion

The approach to quantifying connectivity presented here has three principal advantages to the current frameworks under which connectivity is assessed. First, defining connectivity strength as a metric between 0 and 1 treats connectivity as a continuous variable that can vary through time, which is more representative of how landscape connectivity occurs. This is an improvement over binary or categorical (i.e., connected or isolated) assessments of connectivity, as it is often treated in studies that infer

landscape connectivity from hydrologic time series analysis (16), geomorphic and streamflow thresholds (44) or classifications using clustering approaches (15). Second, the framework presented here can simultaneously quantify both lateral surface connectivity (i.e., between the river Inflow site and the floodplain) and longitudinal connectivity (i.e., upstream and downstream sites along a river) dynamics using the same metrics. This is in contrast to previous studies that defined connectivity in a manner that explicitly fixed a single dimension to connectivity or presented connectivity as a ratio between two dimensions of connectivity (45). Third, our framework enables multiple field-based empirical approaches to quantify connectivity, which allows for the application of connectivity metrics that are best suited for the system being studied.

Connectivity parameters derived from the model fit enabled us to identify three major surface water connectivity regimes operating within the river-floodplain system during the study period (Figure 4). Sites were observed to be either: stable and highly connected (high σ, low Δ); stable and isolated (low σ, low Δ), or intermittently connected (variable σ, high Δ). The stable and highly connected sites were those longitudinally connected along the main stem of the river. Interestingly, even these sites exhibited evidence of a small shift toward decreased connectivity strength at or near base flow (Figure 2). The only site to demonstrate stable and isolated behavior was the site Pond-Iso where we observed no surface connection to the main channel and consistently had low connectivity strength values despite being geographically near the river main stem, demonstrating that geographic proximity does not dictate high hydrologic connectivity.

At sites with intermittent connectivity regimes, interactions between river flow dynamics and floodplain geomorphic structures generated variability in the timing and speed of changes in connectivity. Our analyses suggest much of the floodplain became disconnected from the main stem of the river during the falling limb in response to declines in river stage between June 18 to July 04 (Figure 1 & 3). However other sites including Pond-Con-01 and Main-Braid disconnected later during the recession period suggesting variability in the physical thresholds that must be exceeded to enable lateral surface flow (Figure 4). Most of the sites that disconnected during the falling limb exhibited fast changes (high *v* values) that occurred within 1-14 days suggesting that when stream levels dropped below a specific threshold, these sites rapidly shifted to a disconnected state. The high uncertainty observed for *v* at these sites may be because the one week sampling interval was not frequent enough to accurately describe the rate of disconnection. Accordingly, sampling designs need to be aligned with the temporal dynamics of the system being studied. For example, flashy hydrologic systems where water levels rise and fall very quickly will require fine resolution sampling that matches the temporal dynamics of the process. However, at other sites including Pond-Con-01, Main-Braid and Side-01, the shifts were gradual (low *v* values) taking more than three weeks for sites to reach a new disconnected stable state. We were unable to distinguish the mechanisms for these more gradual shifts with our current study design. Low *v* values may have been driven by gradual reductions in river water flows relative to other water sources, or some sites may have integrated behavior of multiple flowpaths that disconnect at different times.

Estimations of connectivity strength derived from our framework were supported by the two injection experiments (Table 1). During the high flow tracer injection, we observed tracer arrival at all of the sites that had high connectivity strengths (range: σ_g: 0.57- 0.70, σ_m: 0.64-0.84). Conversely, we observed no tracer arrival at Pond-Iso, which had low connectivity scores (σ_g: 0.33, σ_m: 0.17). During the intermediate flow tracer injection, we only observed tracer arrival at the two main stem channel sites, which were also the only two sites that had high connectivity strength (range: σ_g: 0.63- 0.77, σ_m: 0.73-0.75) at the time of the injection experiment. Conversely, at all other sites we observed no tracer arrival during the intermediate flow injection, which was consistent with measured low connectivity strength values (range: σ_g: 0.25- 0.52, σ_m: 0.24-0.39) (Table 1, Figure 2).

7.1 Characterization of the microbiome as an indicator for hydrologic connectivity

We hypothesized that characteristics of each site's microbiome could be used to infer hydrologic connectivity. Our results demonstrated strong general agreement between microbiome membership and hydrologic and geochemical indicators of connectivity. Microbiome membership was highly responsive to connectivity between the Inflow site and each target site. At high flow conditions, there was substantial hydrological connectivity across the river-floodplain systems and water column microbiome membership at multiple target sites within the floodplain was similar to those at the Inflow site. However, as flows decreased microbiome membership at many target sites rapidly became dissimilar from the Inflow site. Further, the directionality of how microbiomes diverged from the Inflow site varied among sites (Figures S1 & S2). These between-site differences were likely driven in part by hydrologic factors such as distance along surface flow paths, residence times of flow paths, and contributions of other source waters and their associated microbiome. In addition, differences among each site's environment are also likely to influence membership distinctly. Microbial communities are shaped not just by dispersal but also by local ecological dynamics that come to dominate microbiome assembly as residence time becomes greater than growth rate (46). As flow decreases and residence times increase in a water body, selection driven by local environmental conditions is likely to become a larger factor relative to dispersal (i.e., immigration and emigration) in determining microbiome membership (47), which could result in increasing dissimilarity between a source and target location.

This shift towards a selection driven microbial community assembly may only be observable when residence times increase above a certain threshold, which might help explain the discrepancy in timing of connectivity shifts observed at Pond-Con-01 between the microbial and geochemical connectivity metrics (Figure 2 & 4). At Pond-Con-01, the connectivity strength estimated by microbiome membership (σ_m) began to decline gradually during the falling limb as river flow declined. This preceded a decline in the connectivity strength estimated by geochemical composition (σ_g) by approximately forty days, which declined at the same time as stage in the pond began

falling. Pond-Con-01 was located along a lateral surface flowpath that passed through several beaver ponds before reaching the site. As a result, even at peak river flows, water velocities through Pond-Con-01 were low, and travel times were long, relative to other sites (Table 1). As river flow declined during the falling limbs, residence times increased as inflows to the pond declined but pond levels and volume remained stable. Through this period, the stable levels and persistence of high geochemical connectivity strength suggest a surface connection to the river was maintained, but the degree of influence of the river on the pond microbiome declined. As we only observe this behavior at a single site, we suggest a key next step to applying the microbial connectivity metric (σ_m) more widely will be identifying how residence time thresholds in different systems and applications interact with microbial membership.

7.2 Quantifying Spatiotemporal Variability in Hydrologic Connectivity

Improved quantitative assessment of hydrologic connectivity dynamics across differing systems will enhance our ability to interpret and predict complex system behavior. By treating connectivity strength as a continuous variable, we can characterize hydrologic connectivity as a distribution of connectivity strengths with spatial and temporal dimensions (Figure 3). Quantifying connectivity in a spatiotemporal context will improve our ability to predict the net effects of complex landscape components on downstream waters. Assessing connectivity in a spatiotemporal context is also critical for identifying control points in a landscape that may have disproportionate influence on hydrologic and biogeochemical properties of the ecosystem (48). In watershed scale studies that investigate upland to stream connectivity (49) this approach could help rank the relative contributions of differing hillslopes (i.e., uplands) on processes such as streamflow generation and solute export. In ecological studies that link connectivity to biodiversity (3), habitats can be better described by quantifying distributions of their hydrologic connectivity with other components in their landscape.

8. Summary

We developed and tested a framework to assess hydrologic connectivity between a source and target site within a landscape using field based indicators. The framework provides the ability to move beyond binary assessment of connectivity and quantify spatial and temporal distributions of connectivity. This approach generates a deeper understanding into the variability of landscape scale hydrologic processes. We illustrate the utility of this approach within a montane river-floodplain system by quantifying the presence, stability and timing of surface connectivity and disconnectivity between the river Inflow and sites located both longitudinally down river and laterally on the floodplain during the snowmelt hydrograph recession. While the specific indicators of connectivity may vary among systems, quantifying common parameters and spatiotemporal distributions to describe the connectivity regime of landscapes within this framework will facilitate inter-system comparisons.

Our work also demonstrates that aquatic microbiomes can be utilized for inference into hydrologic connectivity. By examining similarity in microbial membership, we accurately assessed the presences/absences of surface flows from the main channel. We also find preliminary evidence that aquatic microbiomes can provide additional information on residence time dynamics along connected flow paths. Further efforts are needed to test how this metric operates within differing temporal and spatial scales. We also suggest that future work implement finer-scale OTU-level analysis rather than a coarse community level similarity metric, which we believe can increase the ability to detect weaker flow paths and potentially be used as a multi-tracer to simultaneously measure numerous sources of connectivity.

9. Acknowledgements

We thank Connor Lockwood for field assistance and Tim Fegel and Kristen Otto for lab assistance, and Rocky Mountain National Park for site access and the Rocky Mountain Research Station for use of their lab facilities. This work was funded by National Science Foundation EAR #1632798, Department of Energy grant #0000241776, and a NASA National Earth and Space Science Fellowship awarded to Alex Brooks. Data and relevant scripts will be made publically available on CUAHSI Hydroshare Repository upon publication.

10. References

1. L. J. Bracken, *et al.*, Concepts of hydrological connectivity: Research approaches, Pathways and future agendas. *Earth-Science Rev.* **119**, 17–34 (2013).
2. T. Covino, Hydrologic connectivity as a framework for understanding biogeochemical flux through watersheds and along fluvial networks. *Geomorphology* **277**, 133–144 (2017).
3. C. Amoros, G. Bornette, Connectivity and biocomplexity in waterbodies of riverine floodplains. *Freshw. Biol.* **47**, 761–776 (2002).
4. S. G. Leibowitz, *et al.*, Connectivity of Streams and Wetlands to Downstream Waters: An Integrated Systems Framework. *J. Am. Water Resour. Assoc.* **54**, 298–322 (2018).
5. J. V. Ward, The Four-Dimensional Nature of Lotic Ecosystems Author (s): J . V . Ward Source : Journal of the North American Benthological Society , Vol . 8 , No . 1 (Mar ., 1989), Published by : The University of Chicago Press on behalf of the Society for Freshwa. *J. North Am. Benthol. Soc.* **8**, 2–8 (1989).
6. M. C. Rains, *et al.*, Geographically isolated wetlands are part of the hydrological landscape. *Hydrol. Process.* **30**, 153–160 (2016).
7. M. J. Cohen, *et al.*, Do geographically isolated wetlands influence landscape functions? *Proc. Natl. Acad. Sci. U. S. A.* **113**, 1978–1986 (2016).
8. F. Y. Cheng, N. B. Basu, Biogeochemical hotspots: Role of small water bodies in landscape nutrient processing. *Water Resour. Res.* **53**, 5038–5056 (2017).
9. D. L. McLaughlin, D. A. Kaplan, M. J. Cohen, A significant nexus: Geographically isolated wetlands influence landscape hydrology. *Water Resour. Res.* **50**, 7153–7166 (2014).
10. L. J. Bracken, J. Croke, The concept of hydrological connectivity and its contribution to understanding runoff-dominated geomorphic systems. *Hydrol. Process.* **21**, 1749–1763 (2007).
11. G. Ali, C. Oswald, C. Spence, C. Wellen, The T-TEL Method for Assessing Water, Sediment, and Chemical Connectivity. *Water Resour. Res.*, 634–662 (2018).
12. K. M. Fritz, *et al.*, Physical and Chemical Connectivity of Streams and Riparian Wetlands to Downstream Waters: A Synthesis. *JAWRA J. Am. Water Resour. Assoc.* (2018) https:/doi.org/10.1111/1752-1688.12632.
13. L. Turnbull, J. Wainwright, R. E. Brazier, A conceptual framework for understanding semi-arid land degradation: ecohydrological interactions across multiple-space and time scales. *Ecohydrology* **1**, 23–34 (2008).
14. A. Cabezas, M. Gonzalez-Sanchís, B. Gallardo, F. A. Comín, Using continuous surface water level and temperature data to characterize hydrological connectivity in riparian wetlands. *Environ. Monit. Assess.* **183**, 485–500 (2011).

15. C. N. Jones, D. T. Scott, B. L. Edwards, R. F. Keim, Perirheic mixing and biogeochemical processing in flow-through and backwater floodplain wetlands. *Water Resour. Res.* **50**, 7394–7405 (2014).

16. M. Rinderer, G. Ali, L. G. Larsen, Assessing structural, functional and effective hydrologic connectivity with brain neuroscience methods: State-of-the-art and research directions. *Earth-Science Rev.* **178**, 29–47 (2018).

17. E. Wohl, *et al.*, Connectivity as an emergent property of geomorphic systems. *Earth Surf. Process. Landforms* **44**, 4–26 (2019).

18. S. P. Good, D. R. Urycki, B. C. Crump, Predicting Hydrologic Function With Aquatic Gene Fragments. *Water Resour. Res.* **54**, 2424–2435 (2018).

19. N. Martínez-Carreras, *et al.*, Hydrological connectivity inferred from diatom transport through the riparian-stream system. *Hydrol. Earth Syst. Sci.* **19**, 3133–3151 (2015).

20. L. Pfister, J. J. Mcdonnell, S. Wrede, P. Matgen, F. Fenicia, The rivers are alive : on the potential for diatoms as a tracer of water source and hydrological connectivity. **2845**, 2841–2845 (2009).

21. D. R. Nemergut, *et al.*, Patterns and Processes of Microbial Community Assembly. *Microbiol. Mol. Biol. Rev.* **77**, 342–356 (2013).

22. B. C. Crump, L. A. Amaral-zettler, G. W. Kling, Microbial diversity in arctic freshwaters is structured by inoculation of microbes from soils. **6**, 1629–1639 (2012).

23. S. Amalfitano, *et al.*, Groundwater geochemistry and microbial community structure in the aquifer transition from volcanic to alluvial areas. *Water Res.* **65**, 384–394 (2014).

24. E. S. Lindström, M. Forslund, G. Algesten, A. K. Bergström, External control of bacterial community structure in lakes. *Limnol. Oceanogr.* **51**, 339–342 (2006).

25. D. S. Read, *et al.*, Catchment-scale biogeography of riverine bacterioplankton. *ISME J.* **9**, 516–526 (2014).

26. D. Savio, *et al.*, Bacterial diversity along a 2600km river continuum. *Environ. Microbiol.* **17**, 4994–5007 (2015).

27. B. C. Crump, J. E. Hobbie, Synchrony and seasonality in bacterioplankton communities of two temperate rivers. *Limnol. Oceanogr.* **50**, 1718–1729 (2005).

28. L. R. Thompson, *et al.*, A communal catalogue reveals Earth's multiscale microbial diversity. *Nature* **551**, 457–463 (2017).

29. J. D. Hewlett, A. R. Hibbert, Factors affecting the response of small watersheds to precipitation in humid areas. *For. Hydrol.* **1**, 275–290 (1967).

30. F. Nippgen, B. L. McGlynn, R. E. Emanuel, The spatial and temporal evolution of contributing areas. *Water Resour. Res.* **51**, 4550–4573 (2015).

31. K. G. Jencso, B. L. McGlynn, M. N. Gooseff, K. E. Bencala, S. M. Wondzell, Hillslope hydrologic connectivity controls riparian groundwater turnover: Implications of catchment structure for riparian buffering and stream water sources. *Water Resour. Res.* **46**, 1–18 (2010).

32. W. Junk, P. B. Bayley, R. E. Sparks, The flood pulse concept in river-floodplain-systems. *Can. J. Fish. Aquat. Sci.* **106**, 110–127 (1989).

33. K. Tockner, F. Malard, J. V Ward, An extension of the food pulse concept. *Hydrol. Process.* **2883**, 2861–2883 (2000).

34. A. Cabezas, *et al.*, The effect of anthropogenic disturbance on the hydrochemical characteristics of riparian wetlands at the Middle Ebro River (NE Spain). *Hydrobiologia* **617**, 101–116 (2009).

35. P. Wegener, T. Covino, E. Wohl, Beaver-mediated lateral hydrologic connectivity, fluvial carbon and nutrient flux, and aquatic ecosystem metabolism. *Water Resour. Res.* **53**, 4606–4623 (2017).

36. D. Laurel, E. Wohl, The persistence of beaver-induced geomorphic heterogeneity and organic carbon stock in river corridors. *Earth Surf. Process. Landforms* **44**, 342–353 (2019).

37. J. G. Caporaso, *et al.*, Global patterns of 16S rRNA diversity at a depth of millions of sequences per sample. *Proc. Natl. Acad. Sci.* **108**, 4516 LP – 4522 (2011).

38. A. E. Parada, D. M. Needham, J. A. Fuhrman, Every base matters: assessing small subunit rRNA primers for marine microbiomes with mock communities, time series and global field samples. *Environ. Microbiol.* **18**, 1403–1414 (2016).

39. A. Apprill, S. McNally, R. Parsons, L. Weber, Minor revision to V4 region SSU rRNA 806R gene primer greatly increases detection of SAR11 bacterioplankton . *Aquat. Microb. Ecol.* **75**, 129–137 (2015).

40. P. D. Schloss, *et al.*, Introducing mothur: Open-Source, Platform-Independent, Community-Supported Software for Describing and Comparing Microbial Communities. *Appl. Environ. Microbiol.* **75**, 7537 LP – 7541 (2009).

41. C. Quast, *et al.*, The SILVA ribosomal RNA gene database project: improved data processing and web-based tools. *Nucleic Acids Res.* **41**, D590–D596 (2013).

42. P. J. McMurdie, S. Holmes, phyloseq: An R Package for Reproducible Interactive Analysis and Graphics of Microbiome Census Data. *PLoS One* **8**, e61217 (2013).

43. C. Ritz, F. Baty, J. C. Streibig, D. Gerhard, Dose-Response Analysis Using R. *PLoS One* **10**, e0146021 (2016).

44. M. A. Reid, M. C. Reid, M. C. Thoms, Ecological significance of hydrological connectivity for wetland plant communities on a dryland floodplain river, MacIntyre River, Australia. *Aquat. Sci.* **78**, 139–158 (2016).

45. J. Harvey, *et al.*, How Hydrologic Connectivity Regulates Water Quality in River

Corridors. *JAWRA J. Am. Water Resour. Assoc.*, 1–13 (2018).

46. E. S. Lindström, M. P. Kamst-Van Agterveld, G. Zwart, Distribution of typical freshwater bacterial groups is associated with pH, temperature, and lake water retention time. *Appl. Environ. Microbiol.* **71**, 8201–8206 (2005).

47. M. J. Mayr, K. Besemer, A. Sieczko, K. Demeter, P. Peduzzi, Bacterial community composition and function along spatiotemporal connectivity gradients in the Danube floodplain (Vienna, Austria). *Aquat. Sci.* **82** (2020).

48. E. S. Bernhardt, *et al.*, Control Points in Ecosystems: Moving Beyond the Hot Spot Hot Moment Concept. *Ecosystems* (2017) https:/doi.org/10.1007/s10021-016-0103-y.

49. K. G. Jencso, *et al.*, Hydrologic connectivity between landscapes and streams: Transferring reach- and plot-scale understanding to the catchment scale. *Water Resour. Res.* **45**, 1–16 (2009).

Supplementary Information for

A Quantitative Framework to Assess Hydrologic Connectivity

Alexander C. Brooks [1,3]
Tim Covino [2,3]
Ed K. Hall [2,3]

1. Department of Geosciences, Colorado State University, Fort Collins, Colorado, 80524, USA

2. Department of Ecosystem Science and Sustainability, Colorado State University, Fort Collins, Colorado, 80524, USA

3. Natural Resources Ecology Laboratory, Colorado State University, Fort Collins, 80524, USA

Table S1: Geochemistry PCA Eigenvectors and % Variance Explained

Ions	PC1	PC2	PC3	PC4	PC5	PC6
Na	-0.48	0.13	-0.01	0.55	-0.30	-0.59
K	-0.46	0.01	0.42	-0.36	0.63	-0.29
Mg	-0.44	-0.30	-0.39	0.41	0.41	0.48
Ca	-0.40	-0.36	-0.44	-0.60	-0.38	-0.11
Cl	-0.44	0.23	0.51	-0.05	-0.42	0.56
SO4	-0.13	0.84	-0.47	-0.18	0.13	0.06
% Variance Explained	0.62	0.18	0.13	0.05	0.02	0.01

Table S2: Root Mean Square Error of Residuals for Logistic and Null Models.

	Geochemistry		Microbial	
Sites	Logistic	Null	Logistic	Null
Main-Braid	0.095	0.215	0.056	0.181
Main-Mid	0.127	0.159	0.052	0.072
Outflow	0.088	0.094	0.075	0.110
Pond-Con-01	0.050	0.123	0.075	0.187
Pond-Con-02	0.054	0.138	0.084	0.215
Pond-Iso	0.035	0.062	0.052	0.056
Side-01	0.085	0.162	0.033	0.227
Side-02	0.092	0.182	0.102	0.248
Side-03	0.087	0.227	0.053	0.229
Side-04	0.067	0.162	0.094	0.201

Table S3: Logistic Parameters (± standard errors) for Geochemical Metric.

		Geochemistry				
Site	***Site Type***	***c***	***d***	***Δ***	***v***	***e***
Main-Braid	Major Channel	0.27 ± 0.07	0.78 ± 0.03	0.5 ± 0.08	0.11 ± 0.05	223.86 ± 5.86
Main-Mid	Major Channel	0.56 ± 0.06	0.81 ± 0.04	0.24 ± 0.07	0.77 ± 1.04	228.32 ± 3.09
Outflow	Major Channel	0.6 ± 0.04	0.7 ± 0.03	0.1 ± 0.05	0.22 ± 0.33	209.73 ± 14.6
Pond-Con-01	Connected Pond	0.22 ± 0.19	0.63 ± 0.03	0.42 ± 0.19	0.07 ± 0.05	232.98 ± 14.41
Pond-Con-02	Connected Pond	0.37 ± 0.02	0.64 ± 0.02	0.27 ± 0.03	0.44 ± 0.32	178.33 ± 1.97
Pond-Iso	Isolated Pond	0 ± 0.05	0.18 ± 0.01	0.18 ± 0.05	0.15 ± 0.07	245.25 ± 6.89
Side-01	Side Channel	0.34 ± 0.03	0.65 ± 0.04	0.31 ± 0.05	0.19 ± 0.12	185.53 ± 5.29
Side-02	Side Channel	0.38 ± 0.03	0.71 ± 0.04	0.34 ± 0.05	0.87 ± 0.85	176.02 ± 1.6
Side-03	Side Channel	0.21 ± 0.04	0.71 ± 0.06	0.51 ± 0.07	0.13 ± 0.1	176.64 ± 3.74
Side-04	Side Channel	0.19 ± 0.02	0.53 ± 0.03	0.34 ± 0.04	0.31 ± 0.23	172.99 ± 2.61

Table S4: Logistic Parameters (± standard errors) for Microbial Metric.

		Microbial				
Site	***Site Type***	***c***	***d***	***Δ***	***v***	***e***
Main-Braid	Major Channel	0.27 ± 0.07	0.8 ± 0.02	0.53 ± 0.08	0.11 ± 0.04	237.79 ± 3.99
Main-Mid	Major Channel	0.67 ± 0.03	0.8 ± 0.02	0.14 ± 0.03	0.22 ± 0.16	231.73 ± 7.1
Outflow	Major Channel	0.63 ± 0.05	0.85 ± 0.03	0.21 ± 0.06	0.1 ± 0.07	217.4 ± 11.02
Pond-Con-01	Connected Pond	0.31 ± 0.05	0.74 ± 0.06	0.43 ± 0.08	0.08 ± 0.05	192.87 ± 6.06
Pond-Con-02	Connected Pond	0.3 ± 0.02	0.72 ± 0.03	0.42 ± 0.04	1.27 ± 1.1	174.36 ± 2.87
Pond-Iso	Isolated Pond	0.25 ± 0.04	0.35 ± 0.01	0.09 ± 0.04	0.17 ± 0.15	236.89 ± 7.94
Side-01	Side Channel	0.37 ± 0.01	0.86 ± 0.01	0.49 ± 0.02	0.21 ± 0.04	182.78 ± 1.13
Side-02	Side Channel	0.27 ± 0.06	0.73 ± 0.06	0.46 ± 0.08	0.61 ± 1.08	180.23 ± 5.4
Side-03	Side Channel	0.25 ± 0.02	0.73 ± 0.02	0.48 ± 0.03	0.7 ± 0.49	175.88 ± 1.19
Side-04	Side Channel	0.29 ± 0.03	0.68 ± 0.04	0.39 ± 0.05	1.01 ± 0.76	172.19 ± 2.29

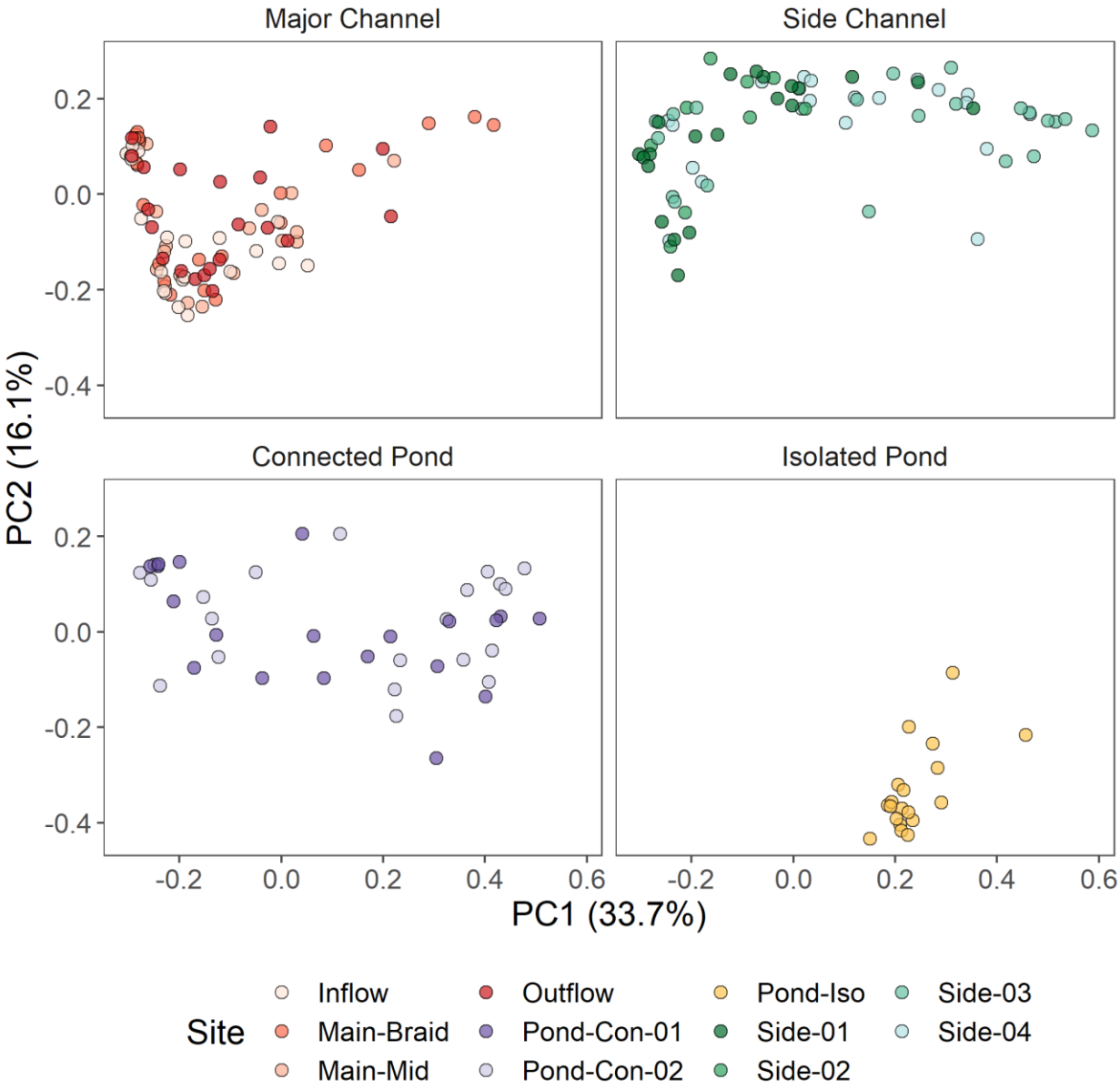

Figure S1: PCOA of Site Microbiomes by Site Type

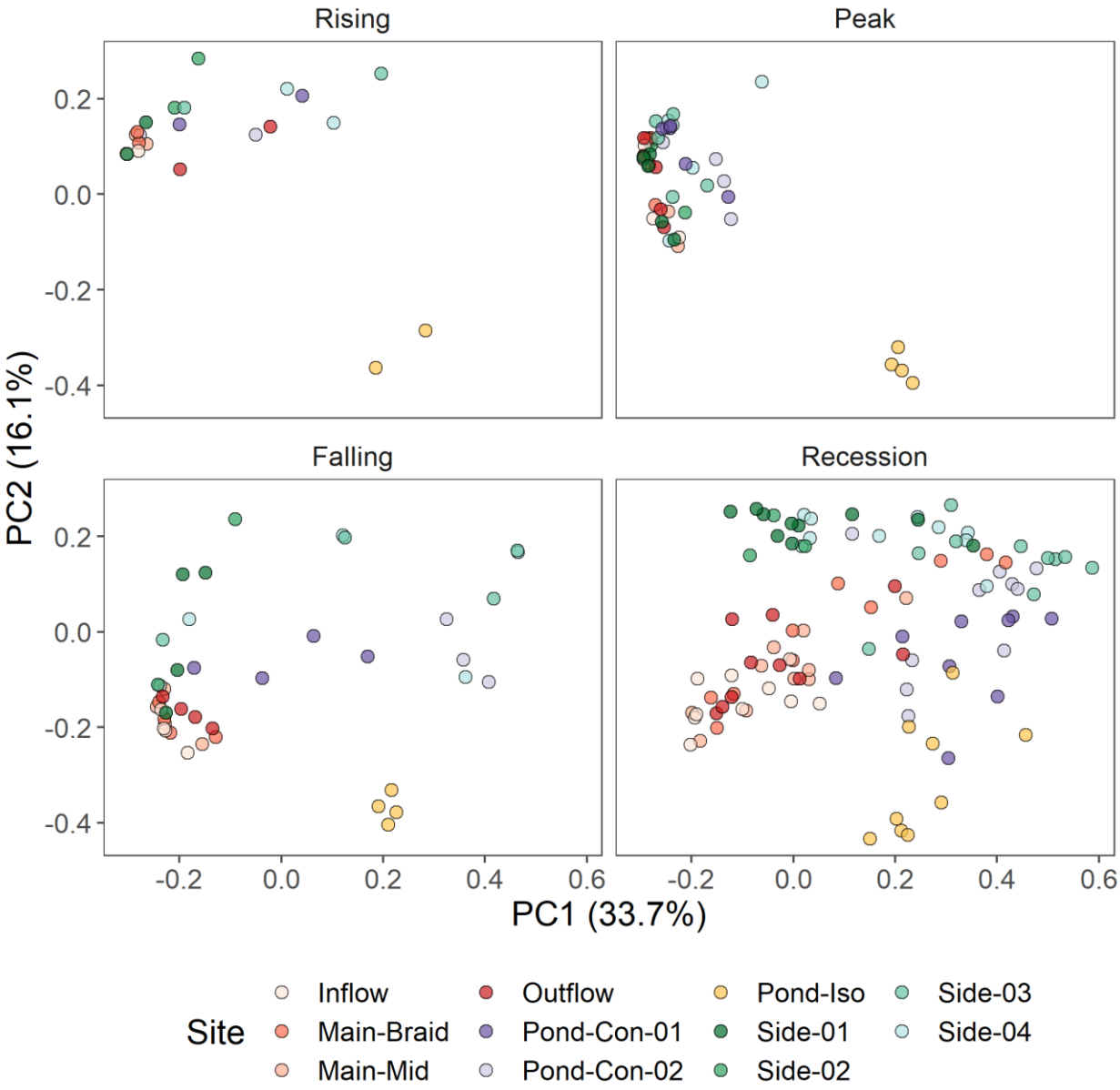

Figure S2: PCOA of Site Microbiomes by Hydro Period

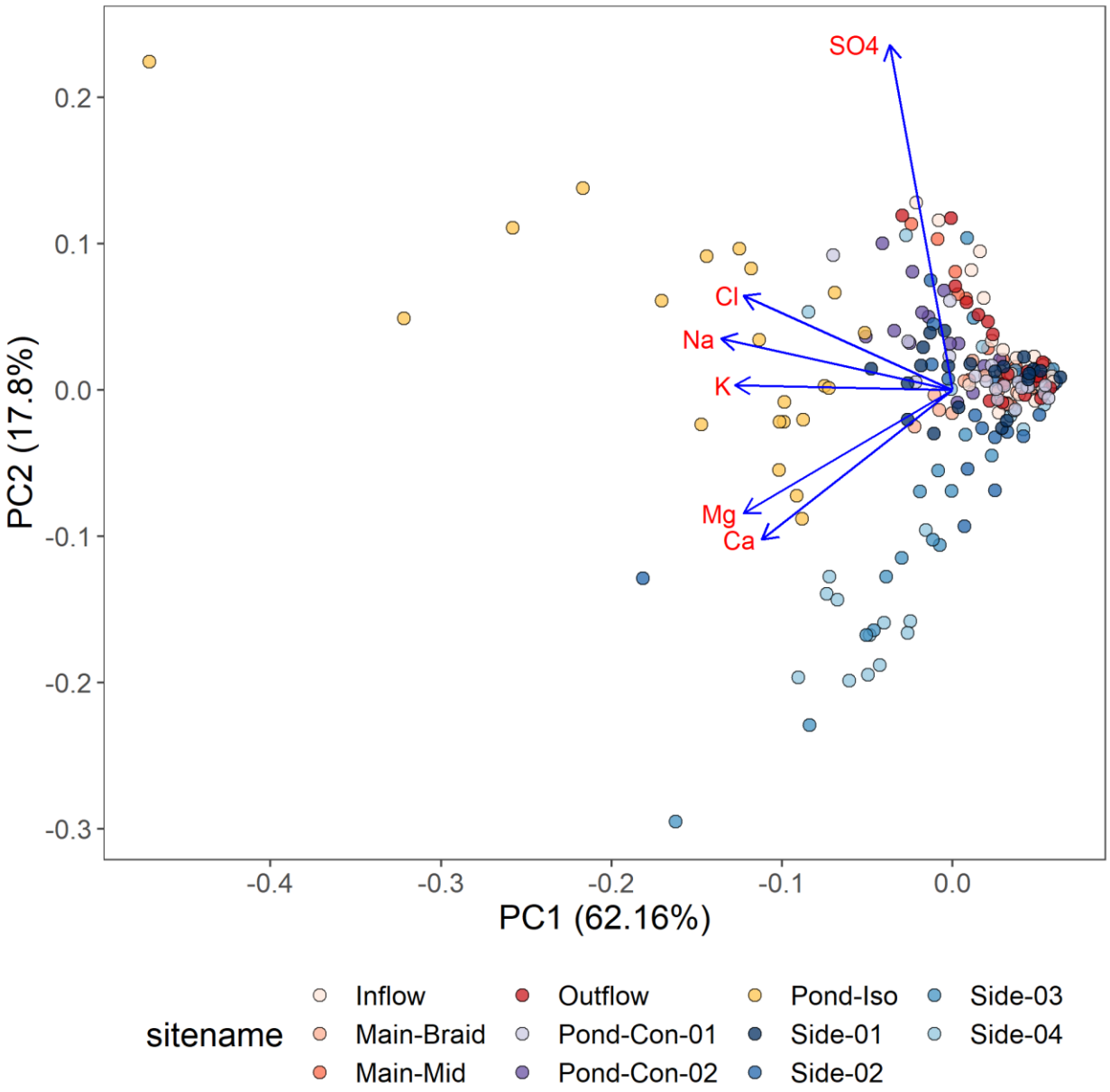

Figure S3: PCA of Geochemical Data with Loadings

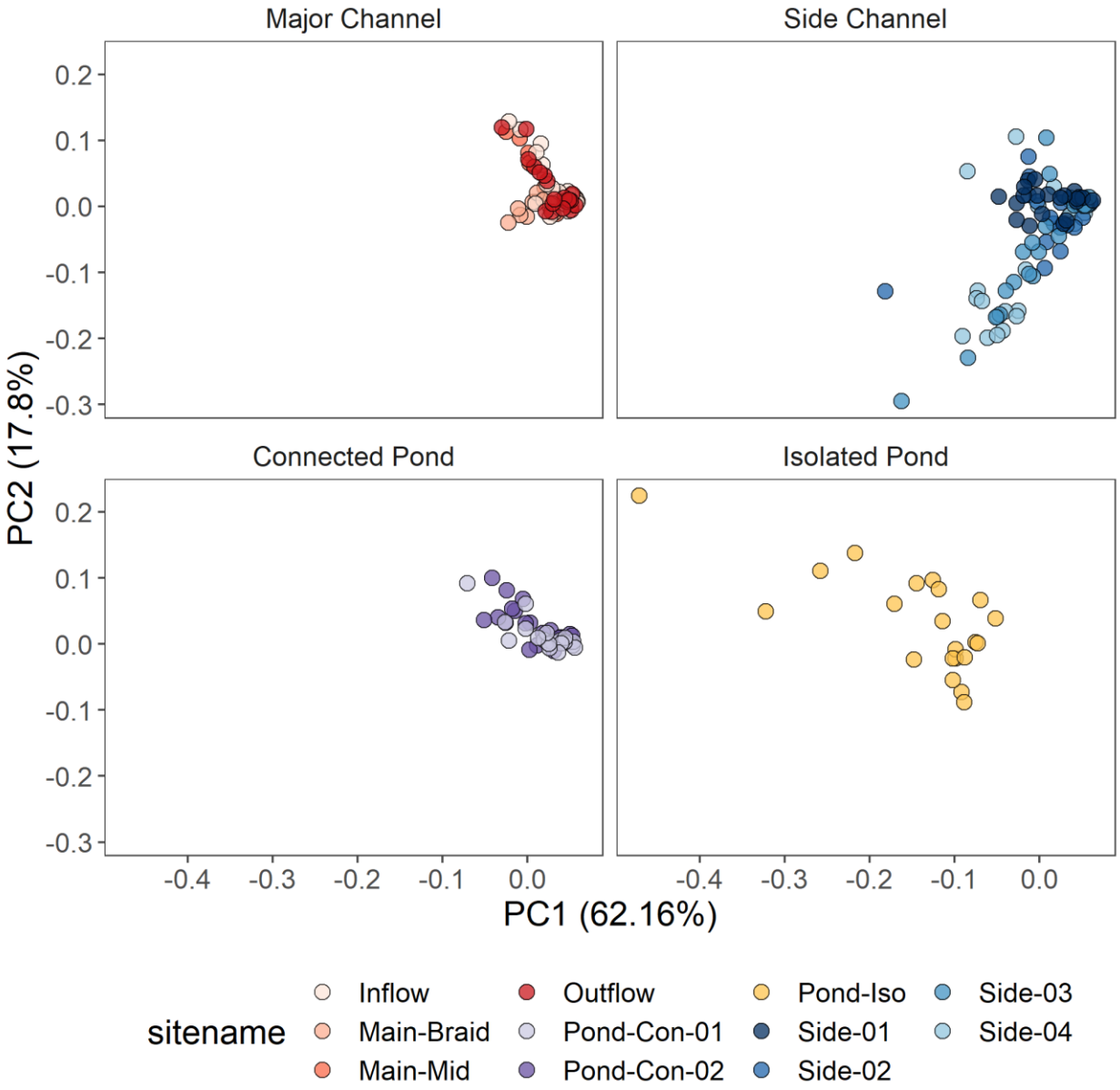

Figure S4: PCA of Geochemical Data by Site Type

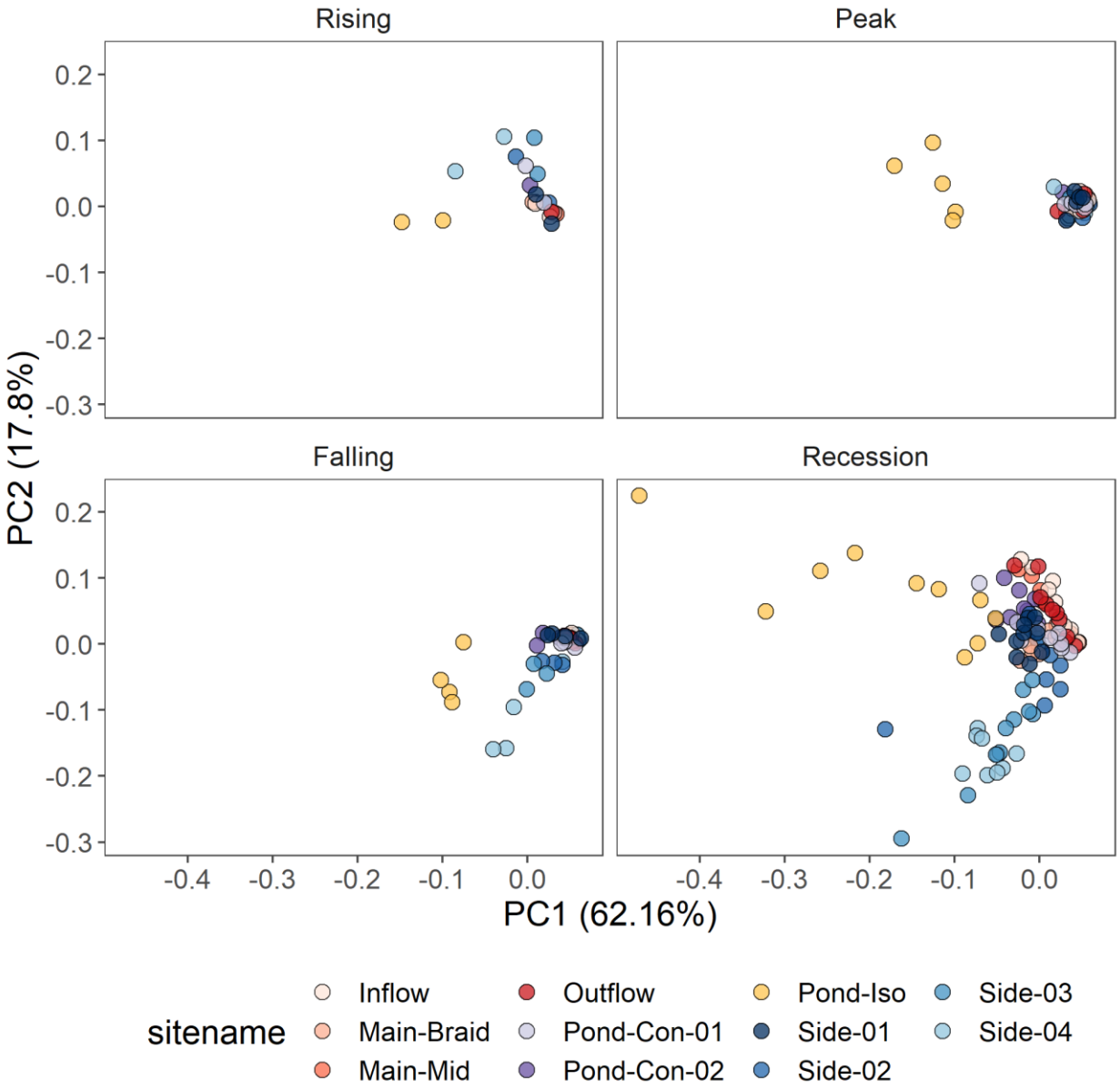

Figure S5: PCA of Geochemical Data by Hydro Period

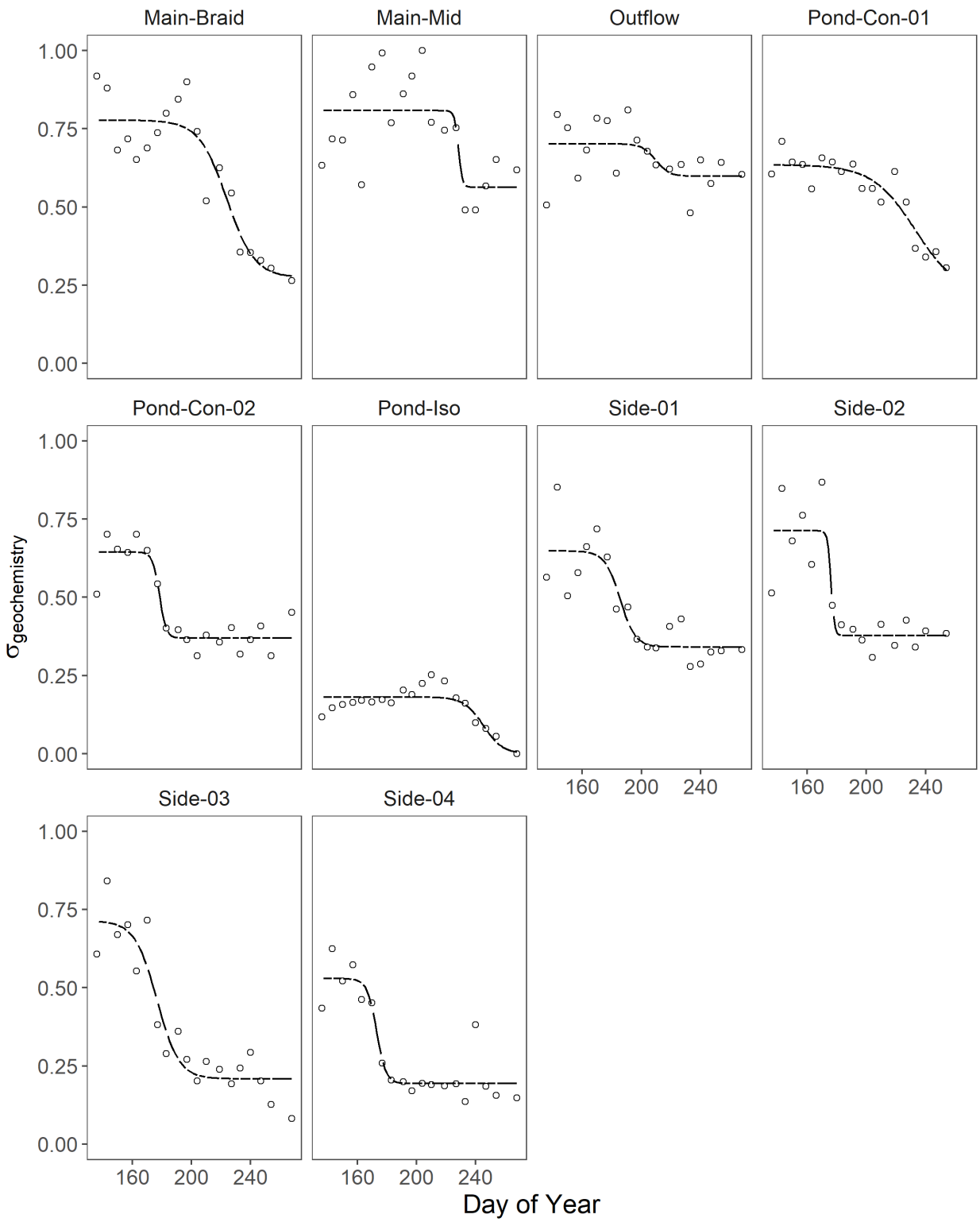

Figure S6: Logistic Curve Fits of Connectivity Strength Derived From Geochemical Metric

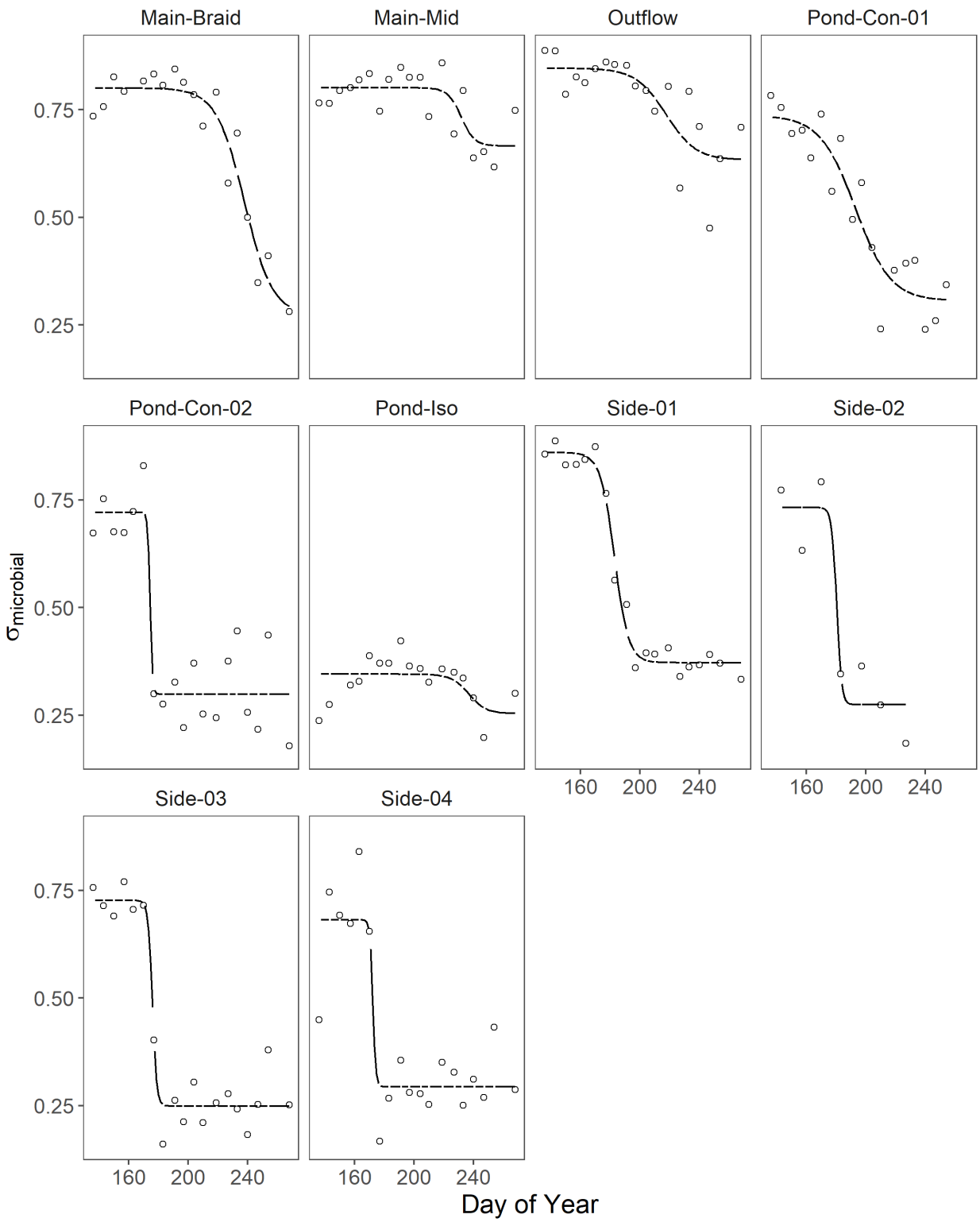

Figure S7: Logistic Curve Fits of Connectivity Strength Derived From Microbial Metric